9-17-2011

Magnetic Analyses of Soils from the Wind River Range, Wyoming, Constrain Rates and Pathways of Magnetic Enhancement for Soils from Semiarid Climates

Emily Quinton
Trinity College, emily.quinton@trincoll.edu

Dennis Dahms
University of Northern Iowa

Christoph Geiss
Trinity College, christoph.geiss@trincoll.edu

Geochemistry Geophysics Geosystems G3

Article
Volume 12, Number 9
17 September 2011
Q07Z30, doi:10.1029/2011GC003728
ISSN: 1525-2027

Published by AGU and the Geochemical Society

Magnetic analyses of soils from the Wind River Range, Wyoming, constrain rates and pathways of magnetic enhancement for soils from semiarid climates

Emily E. Quinton
Environmental Science Program, Trinity College, 300 Summit Street, Hartford, Connecticut 06106, USA

Dennis E. Dahms
Department of Geography, University of Northern Iowa, 127 Sabin Hall, Cedar Falls, Iowa 50614, USA

Christoph E. Geiss
Environmental Science Program and Department of Physics, Trinity College, 300 Summit Street, Hartford, Connecticut 06106, USA (christoph.geiss@trincoll.edu)

[1] In order to constrain the rate of magnetic enhancement in soils, we investigated modern soils from five fluvial terraces in the eastern Wind River Range, Wyoming. Profiles up to 1.2 m deep were sampled in 5-cm intervals from hand-dug pits or natural riverbank exposures. Soils formed in fluvial terraces correlated to the Sacajawea Ridge (730–610 ka BP), Bull Lake (130–100 ka BP) and Pinedale-age (~20 ka BP) glacial advances. One soil profile formed in Holocene-age sediment. Abundance, mineralogy, and grain size of magnetic minerals were estimated through magnetic measurements. Magnetic enhancement of the A-horizon as well as an increase in fine-grained magnetic minerals occurred mostly in Bull Lake profiles but was absent from the older profile. Such low rates of magnetic enhancement may limit the temporal resolution of paleosol-based paleoclimate reconstructions in semiarid regions even where high sedimentation rates result in multiple paleosols. A loss of ferrimagnetic and an increase in antiferromagnetic minerals occurred with age. Our findings suggest either the conversion of ferrimagnetic minerals to weakly magnetic hematite with progressing soil age, or the presence of ferrimagnetic minerals as an intermediate product of pedogenesis. Absolute and relative hematite abundance increase with age, making both useful proxies for soil age and the dating of regional glacial deposits. All coercivity proxies are consistent with each other, which suggests that observed changes in HIRM and S-ratio are representative of real changes in hematite abundance rather than shifts in coercivity distributions, even though the modified L-ratio varies widely.

Components: 6900 words, 11 figures, 1 table.

Keywords: hematite; magnetic enhancement; pedogenesis.

Index Terms: 1512 Geomagnetism and Paleomagnetism: Environmental magnetism; 1519 Geomagnetism and Paleomagnetism: Magnetic mineralogy and petrology; 1540 Geomagnetism and Paleomagnetism: Rock and mineral magnetism.

Received 25 May 2011; **Revised** 4 August 2011; **Accepted** 8 August 2011; **Published** 17 September 2011.

Quinton, E. E., D. E. Dahms, and C. E. Geiss (2011), Magnetic analyses of soils from the Wind River Range, Wyoming, constrain rates and pathways of magnetic enhancement for soils from semiarid climates, *Geochem. Geophys. Geosyst.*, *12*, Q07Z30, doi:10.1029/2011GC003728.

Theme: Magnetism from Atomic to Planetary Scales: Physical Principles and Interdisciplinary Applications in Geoscience
Guest Editors: B. Moskowitz, J. Feinberg, F. Florindo, and A. Roberts

1. Introduction

[2] Rock-magnetic studies of soils have been successfully applied to a range of questions in geology and soil science. These studies had various goals but use the same measurements to characterize the iron-bearing magnetic minerals present in soils. Some of the first studies [e.g., *Kukla et al.*, 1988] aimed to delineate soil horizons and quantify the degree of soil development in loess-paleosol sequences on the Chinese Loess Plateau. More recently, *Grimley et al.* [2004, 2008] used changes in magnetic susceptibility to delineate the extent of hydric soils. Several authors [e.g., *Grimley et al.*, 2003; *Singer et al.*, 1992; *Vidic et al.*, 2004] have correlated soil age and pedogenic development with the increase in ferrimagnetic mineral concentrations in the upper soil horizons and used these correlations to estimate rates of magnetic enhancement or to constrain the duration of soil development.

[3] Soil-magnetic analyses have also been used to understand the relationship between a given soil profile and its parent material, sediment provenance, and to characterize erosion rates [e.g., *Dearing et al.*, 2001; *Spassov et al.*, 2003]. Correlation between the magnetic signal and precipitation has been used to reconstruct past changes in climate, particularly variations in precipitation [*Han et al.*, 1996; *Heller and Liu*, 1986; *Maher and Thompson*, 1995; *Maher et al.*, 2003b; *Virina et al.*, 2000]. Each of these studies posed questions that often necessitate further study across varied locations and pedogenic conditions. For example, the models and correlations that link magnetic enhancement to climate are specific to a particular region or climatic zone, and the process of magnetic enhancement and its causes are still poorly understood. *Singer and Fine* [1989] examined various pedogenic processes, while others [e.g., *Geiss and Zanner*, 2007; *Maher et al.*, 2003a] correlated modern climate with pedogenic enhancement in modern soils.

[4] *Dearing et al.* [1996] as well as *Blundell et al.* [2009] applied statistical analyses to a large national data set to pinpoint the factors most responsible for magnetic enhancement. Nevertheless, the pathways of magnetic enhancement are still under investigation. In many midlatitude sites, pedogenic magnetite and maghemite formation is the main cause of enhancement [*Maher and Thompson*, 1999; *Orgeira et al.*, 2011, and references therein]. These authors suggest that the formation of pedogenic iron oxide minerals proceeds along two distinct pathways. The precipitation of small ferrimagnetic particles is the result of cyclical changes in soil moisture which cause alternating reducing and oxidizing conditions. Drier climates, however, lead to a more thorough oxidation of iron-bearing precursor minerals and the formation of imperfect antiferromagnetic minerals (hematite or goethite). Balsam and coworkers [*Balsam et al.*, 2004; *Ji et al.*, 2001] determined hematite/goethite ratios for several Chinese loess/paleosol sequences and found that paleosols were enriched in both ferrimagnetic and antiferromagnetic minerals. Hematite formation is favored in warm climates with extreme dry periods that are interrupted only by short precipitation events, while goethite formation predominates under less variable and more humid moisture conditions in soils that have higher organic matter content. According to this model hematite is the predominant pedogenic iron-oxide phase in climates with mean annual precipitation less than 500 mm/yr. *Orgeira et al.* [2011] fine-tune this enhancement model and link the resulting magnetic enhancement to annual changes in soil moisture. Again, hematite production is favored under dry, warm climatic conditions. An alternative magnetic enhancement model has been presented by Barrón and colleagues [e.g., *Barrón and Torrent*, 2002; *Torrent et al.*, 2006] which postulates that magnetic particles form through the oxidation of ferrihydrite to hematite and that ferrimagnetic minerals are merely an intermediate, metastable product in this transformation process, which is not dependent on repeated wetting and drying cycles.

[5] Which of these enhancement models properly describes the development of soil-magnetic properties is, at this point, unclear. Analyses of modern African [*Lyons et al.*, 2010] and Mediterranean [*Torrent et al.*, 2010] soils support the model of

Barrón and Torrent [2002]. However, the timescales required to achieve significant magnetic enhancement (~10^5 years) conflict with observed magnetic enhancement in many modern and Holocene soils [e.g., *Geiss and Zanner*, 2007; *Maher et al.*, 2003b]. Furthermore, the model may have difficulties in explaining the observed abundances of maghemite, hematite, and goethite that have been reported from several loess records [*Maher*, 2011]. In combination with other sites from arid environments the soil profiles analyzed in this study may help to differentiate between these two magnetic enhancement models and strengthen our ability to use soil-magnetic proxies to reconstruct past climatic conditions.

[6] Rates of magnetic enhancement are also poorly constrained. *Singer et al.* [1992], from their study of California beach terraces, concluded that soil ages of up to 100,000 years were required for significant development of ferrimagnetic minerals to occur. *Maher and Hu* [2006], on the other hand, suggested that magnetic minerals might develop rapidly in loessic soils on the Chinese Loess Plateau, which is supported in a recent study by *Geiss et al.* [2009]. Long-term surface soil development can be further complicated by cyclical climate patterns, such as a succession of glacial and interglacial climates [*Hall*, 1999]. In this study, we carefully characterized the magnetic properties of five soil profiles from a chronosequence of the eastern flank of the Wind River Range to estimate rates and pathways of magnetic enhancement for soils that formed over the past <10 ka–730 ka [*Dahms*, 2004] in a semiarid climate.

[7] Determining the rates of magnetic enhancement constrains the temporal resolution that is achievable in paleosol-based climate reconstructions. Soils from semiarid regions may be of additional interest for several reasons: Much of early human history, for example, took place in (now) semiarid regions, and climatic shifts may have influenced the history of early civilizations. Today, agriculture extends into often fragile grassland and steppe regions and is susceptible to short- or long-term climatic change. Paleosols may provide valuable information on the range of past climatic changes, but only if pedogenesis occurs rapidly enough to record short-term (centuries to millennia) climate variations. A better understanding of the chemical processes and pathways that affect magnetic minerals in soils are a prerequisite to understand and model magnetic enhancement and is necessary to interpret the magnetic properties of paleosols in terms of past environmental changes.

[8] The soils analyzed in this study developed in gravel deposits derived from Triassic red beds and are dominated by hematite. They offer the opportunity to investigate the effects of magnetic enhancement on soils from an unusual parent material over time spans up to more than half a million years. In addition, the unusual mineralogy of our sites allows us to compare several magnetic coercivity parameters and establish their reliability as proxies of mineralogical change. Such information aids in the design of robust yet efficient rock-magnetic studies.

2. Methods

2.1. Profile Locations and Site Descriptions

[9] We sampled five soil profiles from fluvial terraces in Red Canyon, 15 km south of Lander, Wyoming (Figure 1). The soils developed in Quaternary gravels derived from the Triassic red beds of the Chugwater group. The soils are mapped as part of the Sinkson-Thermopolis soil association [*Young*, 1981]. They are deep and well drained and contain a well-developed Bky horizon below a depth of approximately 0.4 m depth. Mean annual precipitation for Lander is 230 mm/year with most precipitation occurring during spring and fall. The average annual temperature is approximately 6.5°C, ranging from −7°C during the winter to over 20°C during the summer months (NOAA Satellite and Information Service, 4/27/2011).

[10] Age estimates for these profiles are based on landscape position and range from Holocene, (<10 ka, WIN10B), to Sacajawea Ridge, (730–610 ka, WIN10C). Terrace ages are estimated using terrace heights above modern streams, relative soil development, and correlations to regional soil/terrace chronosequences [*Dahms*, 2004]. Four of the profiles were collected from shallow soil pits (WIN10A, C, D and E) while the WIN10B profile was collected from a natural exposure. All profiles were described in the field following procedures outlined in the Soil Survey Manual [*Soil Survey Division Staff*, 1993].

[11] Samples were collected at 5 cm intervals throughout the upper meter of the profile. The sampling interval was increased to 10 cm for the deeper part of the profiles in WIN10D and WIN10E. In the field, samples were disaggregated by hand, passed through a two-mm sieve and approximately 100 cm^3 of soil was placed in plastic bags for further analysis.

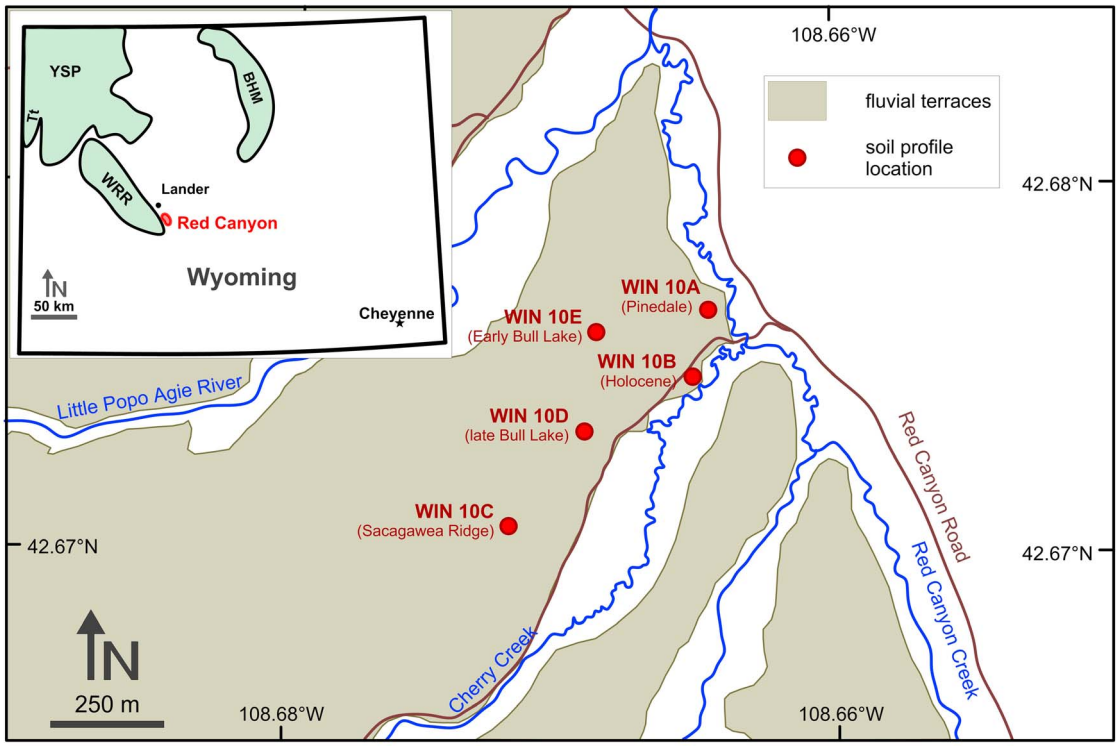

Figure 1. Map of Red Canyon, near Lander, Wyoming, showing the location of the sampled soil profiles. Map insert shows state of Wyoming and location of Red Canyon. BHM – Bighorn Mountains, Tt – Tetons, WRR – Wind River Range, YSP – Yellowstone Plateau.

[12] In the laboratory, samples were air-dried, homogenized and packed into weakly diamagnetic plastic boxes with a volume of 5.3 cm^3. Sample masses ranged between 6.3 and 9.5 g. For high-field analyses, for which we used a vibrating sample magnetometer (VSM), a subset of samples was tightly packed into small gelcaps, which accommodated approximately 0.3–0.4 g of dried sample.

[13] Loss on ignition (LOI) was used to determine inorganic and organic carbon contents for the A- and Bk-horizons of each soil profile. LOI analyses were performed following the procedure of *Dean* [1974]. X-ray diffraction analyses were conducted for representative bulk samples to identify the high-coercivity magnetic mineral component. These analyses were performed using a PANalytical X'pert Pro diffractometer equipped with a rotating sample stage and X'celerator detector.

2.2. Rock-Magnetic Analyses

[14] We performed rock-magnetic analyses to determine the abundance, grain-size and mineralogy of the magnetic minerals present in the soil. All magnetic parameters used in this study are listed in Table 1. We measured mass normalized magnetic susceptibility (χ) using a KLY-4 Kappabridge susceptibility meter. An anhysteretic remanent magnetization (ARM) was imparted in a peak field of 100 mT combined with a 50 μT bias field using a Magnon International AFD 300 alternating field demagnetizer. An isothermal remanent magnetization (IRM) was imparted through three pulses of a 100 mT field using an ASC-Scientific IM-10-30 pulse magnetizer. A saturation IRM (SIRM) was imparted using in three 2.5 T field pulses, followed by a backfield applied in three field pulses of −0.1 T and −0.3 T respectively. All remanence values were measured using an AGICO JR6 spinner magnetometer with a sensitivity of 2×10^{-6} A/m. These measurements were used to calculate S-ratios, as well as the "hard" IRM (see Table 1 for definitions), to estimate the relative and absolute abundance of high-coercivity ("hard") antiferromagnetic minerals, such as hematite or goethite. The modified L-ratio [*Hao et al.*, 2008; *Liu et al.*, 2007, 2010] was also calculated to aid interpretation of S-ratios and HIRM.

[15] Magnetic coercivity distributions were determined through stepwise alternating-field (AF)

Table 1. Magnetic Parameters Used in This Study

Name	Methodology	Magnetic Interpretation
Mass-normalized magnetic susceptibility (χ)	Measured using a KLY-4 Kappabridge susceptibility meter. Units m^3/kg	Provides a rough estimation of the abundance of magnetic minerals in a given sample.
Anhysteretic remanent magnetization (ARM)	Acquired in a peak field of 100 mT and with 50 μT bias field using a Magnon International AFD 300 alternating magnetic field demagnetizer. Units: Am^2/kg	Provides an estimate of the presence of small (0.05–0.06 μm) single-domain (SD) grains; sensitive to both the concentration and grain size of ferrimagnetic minerals.
Isothermal remanent magnetization (IRM_{100mT})	Acquired in three 100 mT field pulses using an ASC-Scientific IM-10-30 pulse magnetizer. Units: Am^2/kg	Estimates the abundance of all remanence-carrying ferrimagnetic (magnetite and maghemite) minerals; relatively independent of grain-size
Saturation isothermal remanent magnetization ($SIRM_{2.5T}$)	Acquired in three 2.5 T field pulses using an ASC-Scientific IM-10-30 pulse magnetizer.	Indicates presence and abundance of all remanence carrying ferrimagnetic and antiferromagnetic (hematite) particles
Backfield IRM IRM_{-100mT} IRM_{-300mT}	Backfield IRM. Acquired following acquisition of SIRM in three pulses of −100 mT and −300 mT, respectively, using an ASC-Scientific IM-10-30 pulse magnetizer.	Used to calculate HIRM and S-ratios (see below)
"Hard" IRM $HIRM_{100}$ $HIRM_{300}$	$HIRM_{-x\,mT} = \frac{1}{2}(SIRM + IRM_{-x\,mT})$	Provides an estimate of the absolute abundance of medium- and high-coercivity magnetic minerals
S-ratio S_{100mT} S_{300mT}	$S_{x\,mT} = -\frac{IRM_{-x\,mT}}{SIRM}$	Provides information on the relative abundance of medium-coercivity SD particles (S_{100mT}) and high-coercivity minerals (S_{300mT})
L-ratio	$L = \frac{HIRM_{300}}{HIRM_{100}}$	Reveals coercivity changes in the antiferromagnetic component; aids in the interpretation of HIRM variations
Magnetic coercivity distributions: AF demagnetization curves DC demagnetization curves	AF demagnetization curves determined through stepwise AF-demagnetization in fields up to 300 mT using Magnon International AFD 300 alternating field demagnetizer. Backfield demagnetization curves were determined using a Princeton Measurement Corporations MicroMag 3900 VSM up to a peak field of 2 T.	Used to constrain the pedogenic component to determine the original of magnetic remanence By reaching a higher peak field the DC demagnetization curves can be used to determine the high-coercivity component, in this case, hematite
Hysteresis loops and coercivity of remanence B_{cr}	Measured using a Princeton Measurement Corporations MicroMag 3900 VSM at a peak field of 1.25 T. B_{cr} determined via single remanence curves.	Hysteresis data provide a general characterization of a sample's bulk magnetic properties, such as magnetic grain size or mineralogy

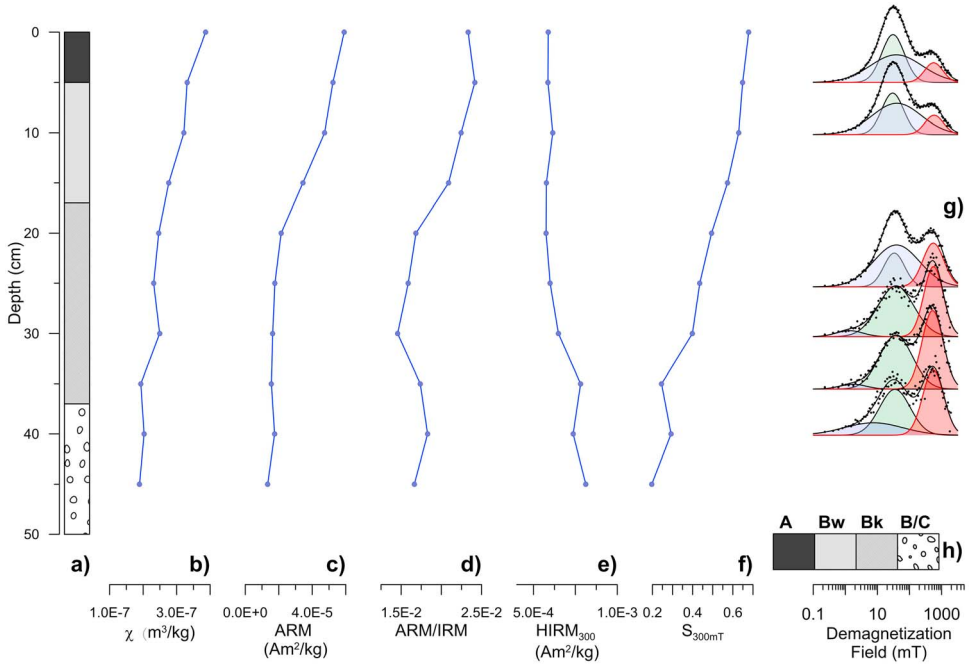

Figure 2. Magnetic properties of (a) soil profile WIN10B (Holocene). The soil profile is located at N42.67514°, W-108.66506°. (b) Magnetic susceptibility (χ), (c) ARM and (d) ARM/IRM are proxies for the abundance of ferrimagnetic minerals. $HIRM_{300}$ and S_{300mT} provide an estimate of the absolute and relative abundance of (e and f) high-coercivity minerals. (g) Magnetic coercivity distributions obtained from backfield demagnetization curves up to 2 T further characterize the nature of the magnetic remanence. There are two components of the magnetic coercivity distributions: a soft component (characterized with two curves) and a hard component. (h) The soil lithology legend applies to Figures 2–6.

demagnetization of an IRM, which was imparted with three field pulses of 1200 mT. The maximum AF demagnetization field was 300 mT. Coercivity data were fitted to cumulative log normal distributions [e.g., *Egli*, 2004; *Robertson and France*, 1994] using the methodology outlined by *Geiss et al.* [2008]. These analyses were performed on a subset of samples.

[16] To characterize bulk magnetic properties, such as saturation magnetization and bulk magnetic grain size, hysteresis loops were measured in applied fields up to 1.25 T using a Princeton Measurements Corporation Model 3900 VSM. Hysteresis data were corrected for para- and diamagnetic contributions using a high-field slope correction. Coercivity of remanence (B_{cr}) was measured through backfield demagnetization in backfields up to 0.2 T.

[17] To extend coercivity distributions to higher demagnetization fields the same subset of samples was given a SIRM in a 2 T field, followed by stepwise backfield (DC) demagnetization. These measurements were carried out using the same VSM. Only DC demagnetization curves are shown because AF demagnetization data do not capture the high-coercivity component present in the soil profiles and both methods yield equivalent information at low fields.

3. Results and Discussion

3.1. Soil Magnetic Properties

[18] Magnetic properties for all studied soil profiles arranged in chronological order, beginning with the Holocene soil profile (WIN 10B, Figure 2) are shown in Figures 2–6. Magnetic susceptibility and IRM are strongly correlated ($n = 75$, $r^2 = 0.98$), therefore, IRM data are not shown. No significant magnetic enhancement occurred in the Holocene soil profile (WIN 10B, Figure 2). The soil developed on a recent fluvial terrace and variations in magnetic properties are predominantly due to changes in parent material.

[19] The Pinedale soil profile (WIN 10A, Figure 3) has higher magnetic susceptibility in the Bk-horizon ($\chi = 8.9 \times 10^{-7}$ m^3/kg) than in the A-horizon

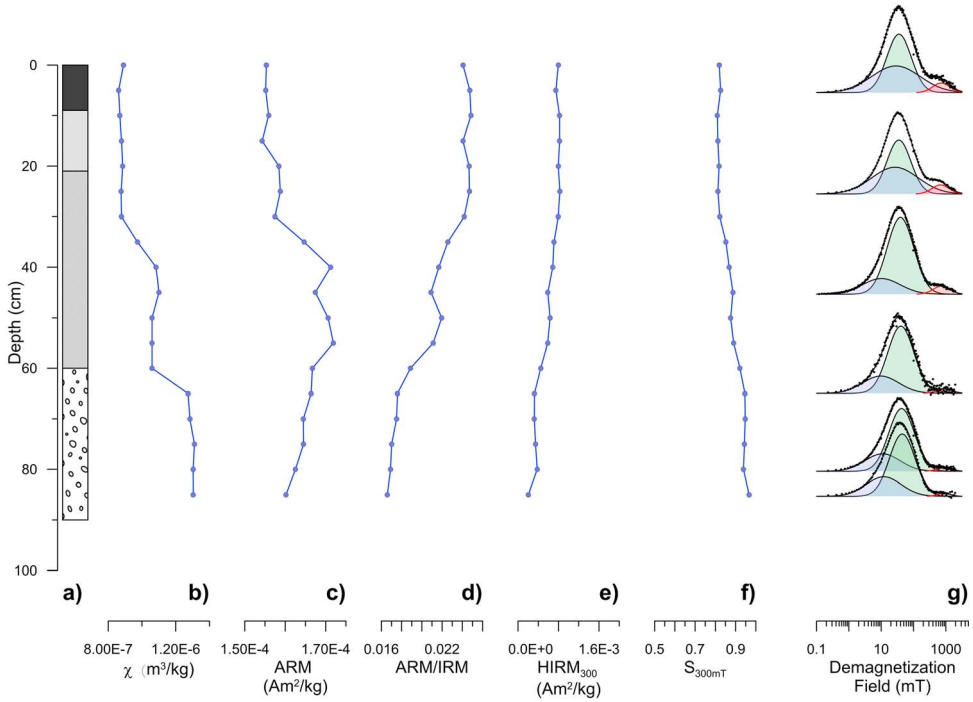

Figure 3. Magnetic properties of soil profile WIN10A (Pinedale, ~20 ka B.P.). The soil profile is located at N42.67708°, W-108.66470°. See caption for Figure 1 for details and soil lithology legend.

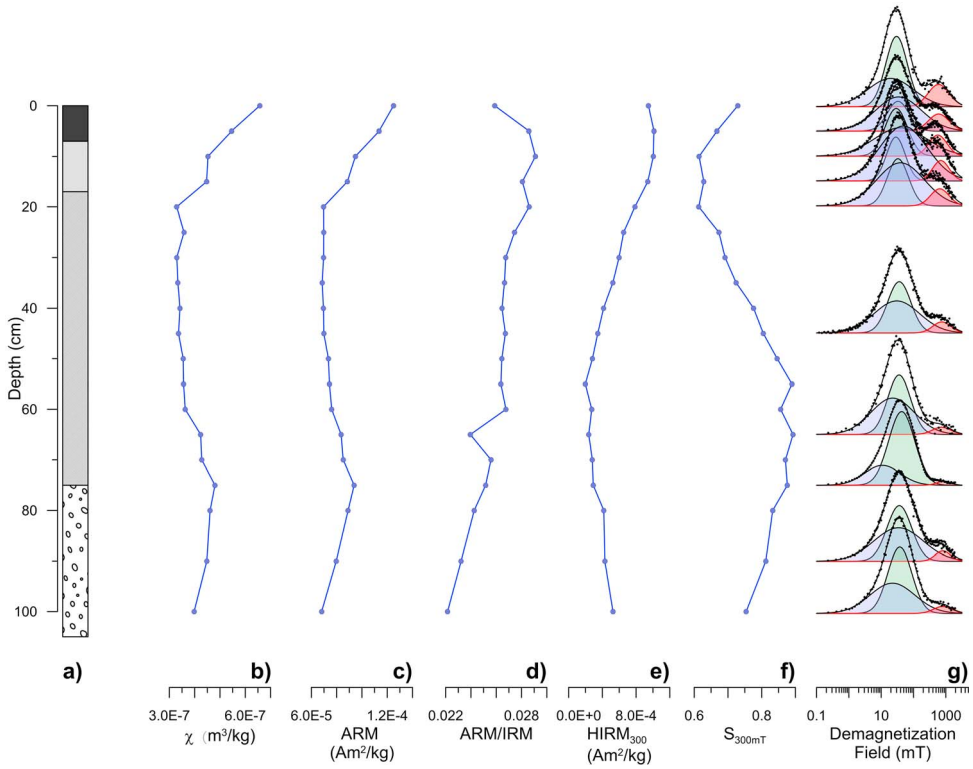

Figure 4. Magnetic properties of soil profile WIN10D (late Bull Lake, ~100 ka B.P.). The soil profile is located at N42.67396°, W-108.66941°. See caption for Figure 1 for details and soil lithology legend.

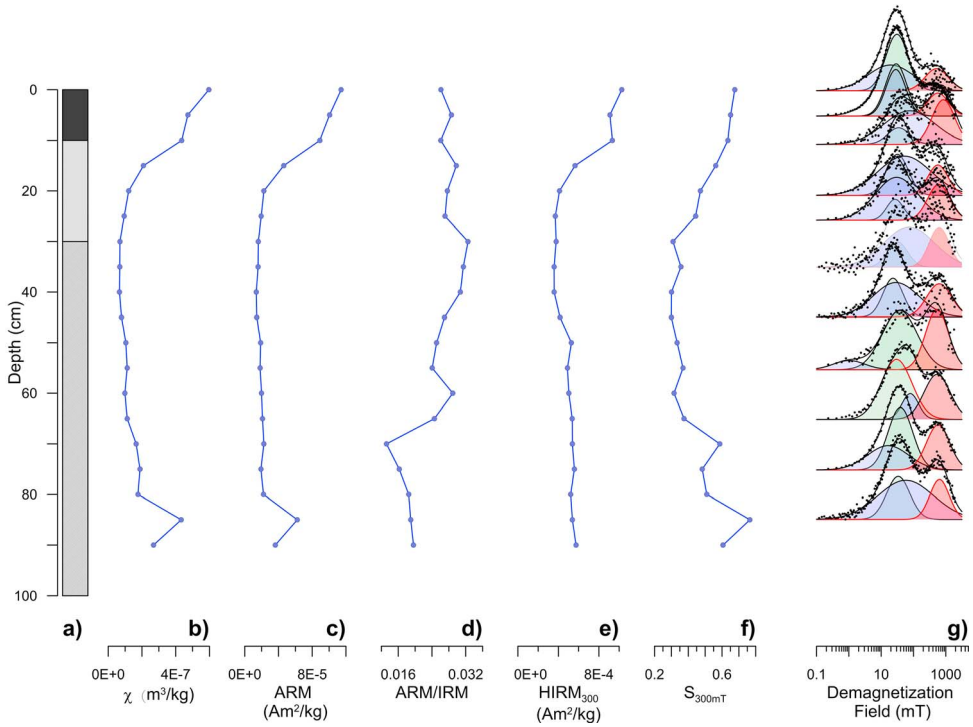

Figure 5. Magnetic properties of soil profile WIN10E (early Bull Lake, ~130 ka B.P.). The soil profile is located at N42.67656°, W-108.66874°. See caption for Figure 1 for details and soil lithology legend.

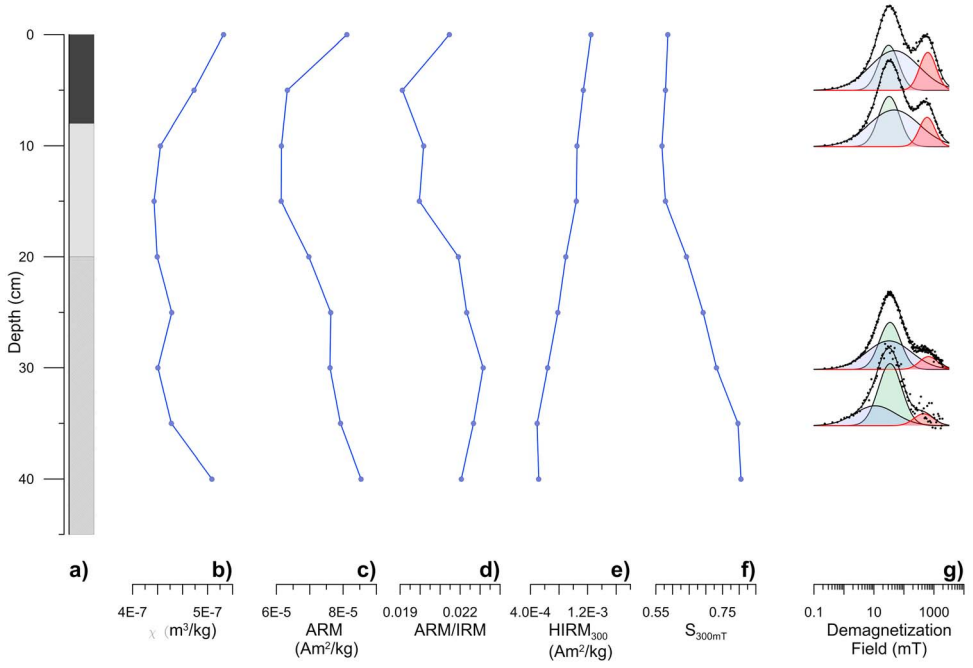

Figure 6. Magnetic properties of soil profile WIN10C (Sacajawea Ridge, 610–730 ka B.P.). The soil profile is located at N42.67134°, W-108.67193°. See caption for Figure 1 for details and soil lithology legend.

($\chi = \times 10^{-7}$ m^3/kg). This may suggest a depletion of ferrimagnetic minerals in the topsoil or the addition of additional, weakly magnetic material to the soil profile. $HIRM_{300}$ and S_{300mT} (Figures 3e and 3f) undergo negligible changes throughout the profile except for a slight decrease in $HIRM_{300}$ with depth and a slight increase in S_{300mT} with depth. Magnetic coercivity distributions (Figure 3g) have a small contribution by hematite to the magnetic remanence (shaded in light red) that is most prominent in the A- and Bk-horizons.

[20] Profiles of Bull Lake age have magnetically enhanced topsoils. For the late Bull Lake soil profile (WIN 10D, Figure 4) moderate enhancement in the A-horizon is suggested by an approximate 100% increase in susceptibility between the Bk-horizon ($\chi = 3.4 \times 10^{-7}$ m^3/kg) and the A-horizon ($\chi = 6.6 \times 10^{-7}$ m^3/kg) (Figure 4b). $HIRM_{300}$ decreases with depth throughout the Bk-horizon while S_{300mT} increases correspondingly. DC demagnetization curves (Figure 3g) indicate increased hematite concentrations (shaded in light red) compared to the Pinedale profile (Figure 2), particularly in the A- and Bw-horizons.

[21] Magnetic enhancement further increases for the A-horizon of the early Bull Lake soil profile (Win 10E, Figure 5). χ increases by almost 1000% between the Bk-horizon ($\chi = 0.66 \times 10^{-7}$ m^3/kg) and the A-horizon ($\chi = 6.0 \times 10^{-7}$ m^3/kg). At this site, $HIRM_{300}$ and S_{300mT} increase in the Bw- and A-horizons (Figures 5e and 5f). Magnetic coercivity distributions indicate a large hematite component throughout the entire profile (Figure 5g).

[22] There is some enhancement of ferrimagnets in WIN10C (Sacajawea Ridge, Figure 6b). χ increases slightly by approximately 20% between the Bk-horizon ($\chi = 4.4 \times 10^{-7}$ m^3/kg) and the A-horizon ($\chi = 5.4 \times 10^{-7}$ m^3/kg). $HIRM_{300}$ increased slightly in the Bw- and A-horizons while S_{300mT} decreased in these horizons (Figures 6e and 6f). Magnetic coercivity distributions indicate an increased hematite component in the Bw- and A-horizons (Figure 6g).

[23] Typical hysteresis loops for two soil samples (A-horizon, WIN10A; Bk-horizon – WIN 10E) are shown in Figures 7a and 7b. Most loops close at magnetic fields above 0.35 T and have a normal shape (neither wasp-waisted nor pot-bellied [*Roberts et al.*, 1995; *Tauxe et al.*, 1996]). A scatterplot of magnetization ratios (M_r/M_s) versus coercivity ratios (B_{cr}/B_c) is shown in Figure 7c [*Day et al.*, 1977; *Dunlop*, 2002]. A-horizon samples (closed symbols) plot in the pseudo-single domain (PSD) field, while Bk-horizon samples (open symbols) are displaced toward higher coercivity ratios. Hysteresis loops from these samples are wasp-waisted (Figure 7b) and close at significantly higher fields. A-horizon samples cluster tightly and do not follow a particular grain size trend. The displacement of Bk-horizon samples may either be due to a larger presence of hematite [*Channell and Mc Cabe*, 1994] or the addition of super-paramagnetic (SP) particles [*Dunlop*, 2002]. If the abundance of SP particles is large, then χ/IRM ratios should also be high, which is not observed in our samples. The presence of hematite is further indicated by the red color of these samples, their wasp-waisted shape, as well as their high magnetic coercivities.

3.2. Magnetic Changes With Soil Age

[24] In Figure 8, various magnetic measurements are plotted as a function of age for typical samples from the A- (solid symbols) and Bk-horizons (open symbols) for all sites with the exception of the Holocene soil profile (whose magnetic properties are controlled by changes in lithology rather than age-dependent pedogenesis). Correcting Bk-horizon data for the presence of carbonates affected the overall magnitude of all concentration-dependent parameters but preserved the trends already observed in the uncorrected data. For clarity these data are omitted from Figure 8.

[25] Concentration-dependent parameters χ (Figure 8a), IRM (not shown) and ARM (Figure 8b) have a decreasing trend with age for the A-horizon. χ remains fairly constant between the two oldest sites (early Bull Lake and Sacajawea Ridge). ARM/IRM ratios (Figure 8c), which increase with age from Pinedale to early Bull Lake, drop again in the Sacajawea Ridge profile. A general increase in B_{cr} values with soil age (Figure 8d) indicates increasing bulk coercivity with soil age. Corresponding trends in HIRM and S_{300mT} indicate that the higher B_{cr} values are due to both an absolute (HIRM increases with age) and relative (S_{300mT} decreases with age) increase of high-coercivity hematite (Figures 8e and 8f). The general decrease in χ and ARM with age in the A-horizons of our soil profiles may be due to a gradual loss of ferrimagnetic minerals or the conversion of ferrimagnetic, or other iron-bearing precursor minerals to weakly magnetic, antiferromagnetic hematite. The increase in ARM/IRM (Figure 8c) for the magnetically enhanced Bull Lake profiles indicates that pedogenic enhancement is at least partially due to an accumulation of SD minerals.

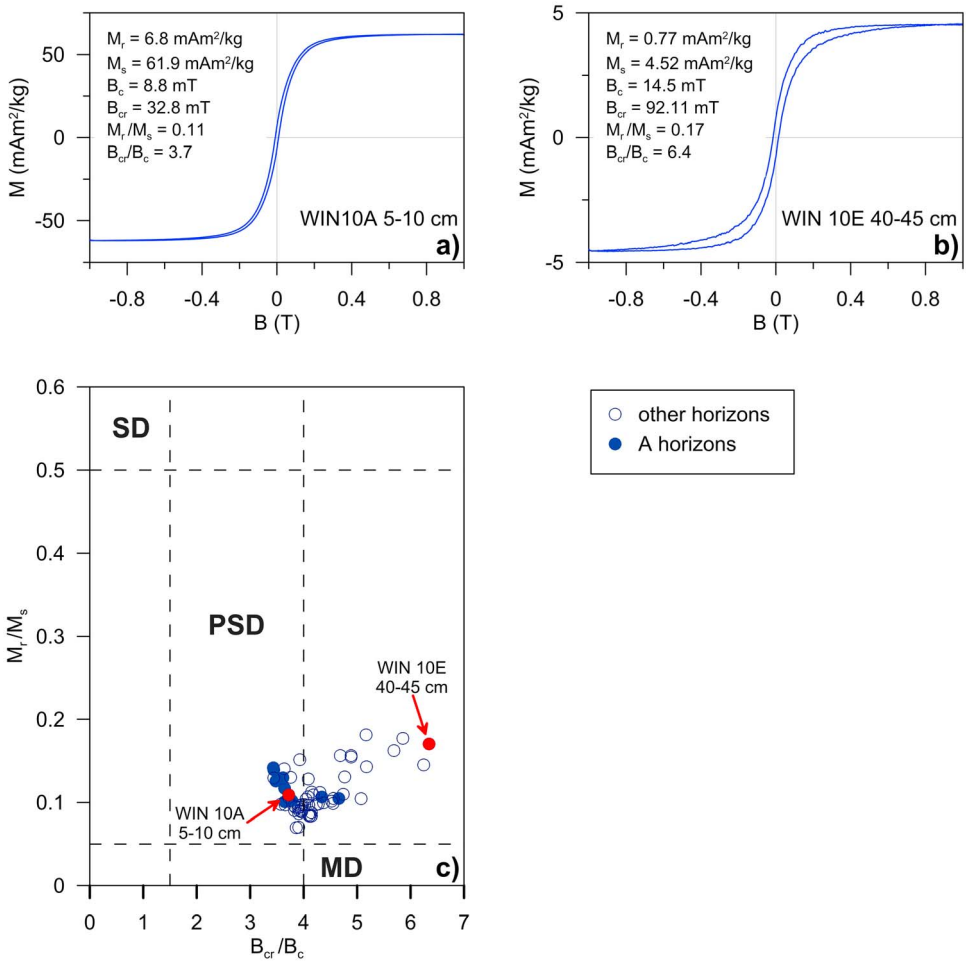

Figure 7. Hysteresis loops for samples (a) WIN10A, 5–10 cm and (b) WIN 10E 40–45 cm. (c) Plot of remanence ratio (M_r/M_s) versus coercivity ratio (B_{cr}/B_c) for all five soil profiles. Solid symbols represent samples from the A-horizon, open symbols represent all other horizons. The positions of the samples shown in Figures 7a and 7b are marked.

[26] In our soil profiles the A-horizons are magnetically enhanced only in the Bull Lake soils (Figures 4 and 5). Based on their investigations of California beach terraces, *Singer et al.* [1992] suggested that little magnetic enhancement is observed in soils younger than approximately 40 ka, which would explain the lack of magnetic enhancement observed in the Holocene and Pinedale soil profiles. The degree of magnetic enhancement increases significantly between the late and early Bull Lake profiles, probably because the early Bull lake soil experienced interglacial climatic conditions during the Sangamon that were more conducive to pedogenic enhancement.

[27] *Hall* [1999] suggested that older soils in the Wind River Basin experienced significant deflation and loss of upper soil horizon material which would strip the older soil profiles of their magnetically enhanced horizons. Magnetic enhancement is a near-surface process and is usually most pronounced in the topsoil. Therefore, long-term deflation can explain the lack of magnetic enhancement in the Sacajawea Ridge soil profile. *Hall* [1999] also found no systematic trend in rubification of the Bt-horizon. We see a systematic change in coercivity parameters with B_{cr} and HIRM increasing and S-ratios declining with age (Figures 8d, 8e, and 8f). Therefore, in contrast to the findings of *Hall* [1999], high-coercivity minerals do systematically increase in the older soil profiles. However, *Hall* [1999] studied Bt-horizons, which are only weakly expressed in our studied soils. Consistent hematite enhancement is only observed in the A-horizons of the soils studied here. Furthermore, increased hematite production may not necessarily lead to further rubification if all grains are either

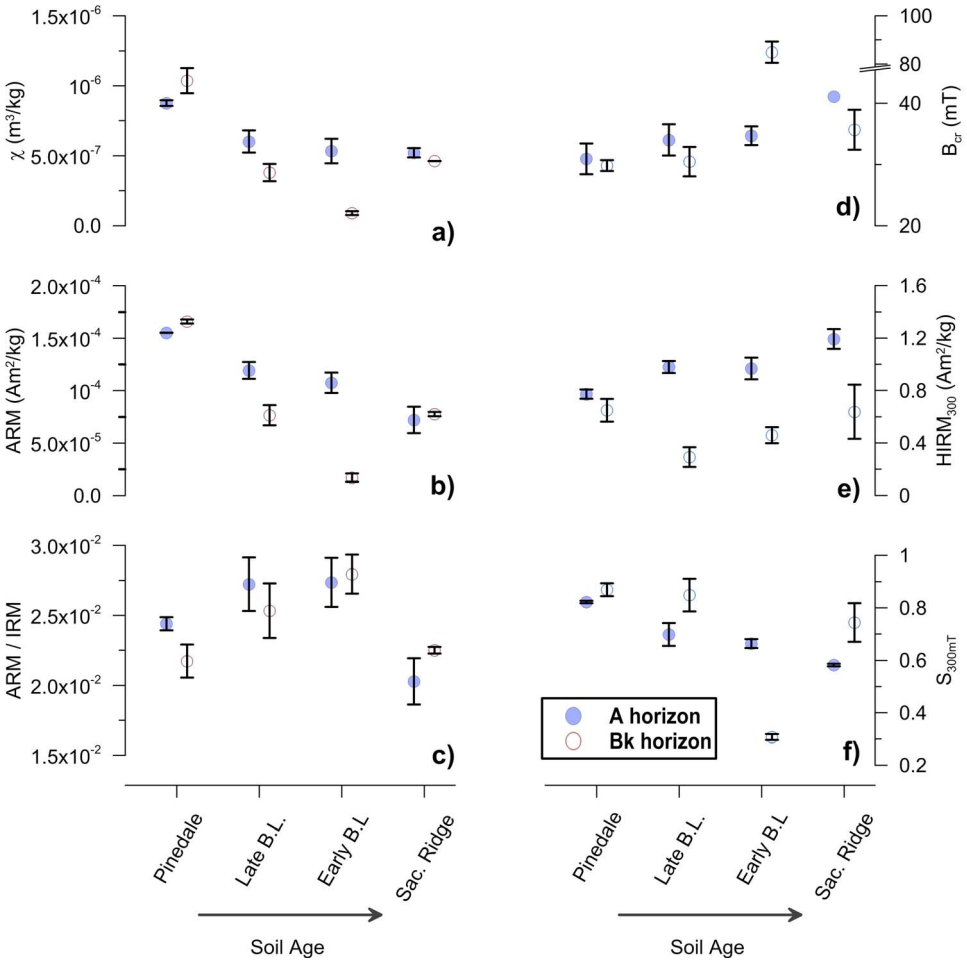

Figure 8. Variations of magnetic properties with age. A-horizon samples: solid symbols, Bk-horizon samples: open symbols.

already completely coated by hematite or if the formation of additional hematite results in enlarging existing hematite crystals rather than the formation of new red material.

[28] To summarize trends in the A-horizons of the studied soil profiles, we observe a loss of ferrimagnetic materials and an increase in hematite. Also, higher ARM/IRM ratios indicate that pedogenic ferrimagnets are created. This suggests that pedogenic ferrimagnets are an intermediate product of pedogenesis with hematite as the stable endmember [*Torrent et al.*, 2006]. In the B-horizons χ, IRM and ARM trends are less clear (Figures 8a, 8b, and 8c). Bk-horizon data do not have consistent trends with age, even when magnetic parameters are corrected for the presence of carbonates. This may be due to the inhomogeneity of the parent material or to complex deflation history, which brings older material closer to the surface.

3.3. Estimates of Hematite Abundance

[29] XRD analyses of representative samples (Figure 9) as well as soil color confirm that the high coercivity component in our soil profiles is carried by hematite. Therefore, estimates of high coercivity distributions can be used to quantify hematite abundance. To assess the consistency of common magnetic coercivity proxies (S-ratio, HIRM and coercivity distributions), we compared relative hematite abundance estimates to S_{300mT} values (Figure 10a). The relationship between these two parameters is fairly linear, which suggests that in our case both methods yield comparable results and can be used to detect qualitative changes in the relative concentrations of high-coercivity minerals. In Figures 10b and 10c the absolute contribution of the high-coercivity component (hematite) to the magnetic remanence as determined by our analysis of magnetic coercivity distributions is plotted against $HIRM_{300}$, an alternative proxy for the absolute

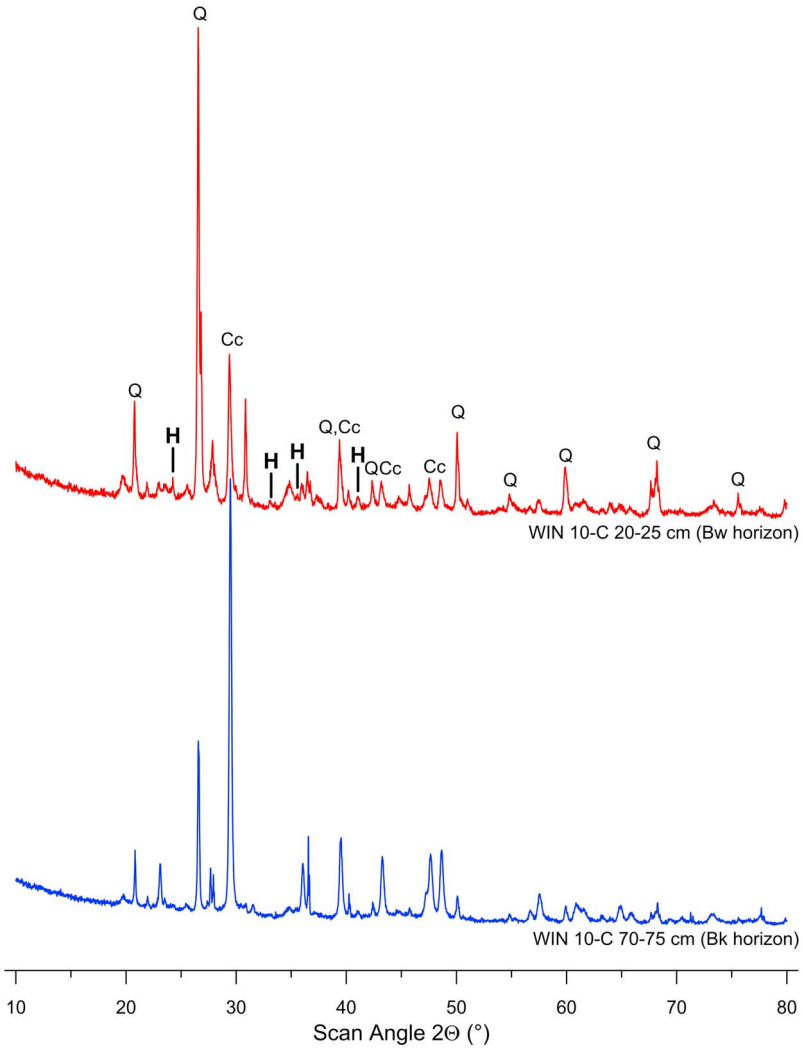

Figure 9. XRD analyses for two representative samples from the Sacajawea Ridge soil profile. Diffraction peaks associated with quartz (Q), calcite (Cc) and hematite (H) are labeled.

hematite abundance. Both parameters have a positive correlation. The correlation between coercivity distribution analyses and HIRM when coercivity spectra are fitted by two coercivity components is shown in Figure 10b. This analysis indicates a good correlation between the two hematite proxies. When coercivity spectra are fitted with three coercivity distributions, often a broad medium-coercivity component is added. This improves the overall fit to the data but the added component overlaps significantly with the remaining low- and high-coercivity components and leads to a poorer correlation between the two proxies (Figure 10c).

[30] *Liu et al.* [2007] introduced the L-ratio (later, the modified L-ratio) to assess the validity of HIRM and S-ratios as proxies for the abundance of high-coercivity minerals (hematite and goethite). According to *Liu et al.* [2007], HIRM only reflects the abundance of high-coercivity minerals if the (modified) L-ratio remains fairly constant, otherwise, changes in HIRM are mainly due to changes in magnetic coercivity. The modified L-ratio is plotted versus $HIRM_{300}$ for all samples in Figure 11a. Considerable variations in the L-ratio have very strong site-specific linear trends. According to *Liu et al.* [2007] the data in Figure 11a suggests that, in our case, HIRM is poorly suited to estimate changes in hematite abundance. *Liu et al.* [2007] suggested a detailed analysis of coercivity distributions (Figures 2–5) to further clarify the contributions of high-coercivity minerals to the magnetic signal because magnetic coercivity spectra do capture changes in magnetic coercivity more completely

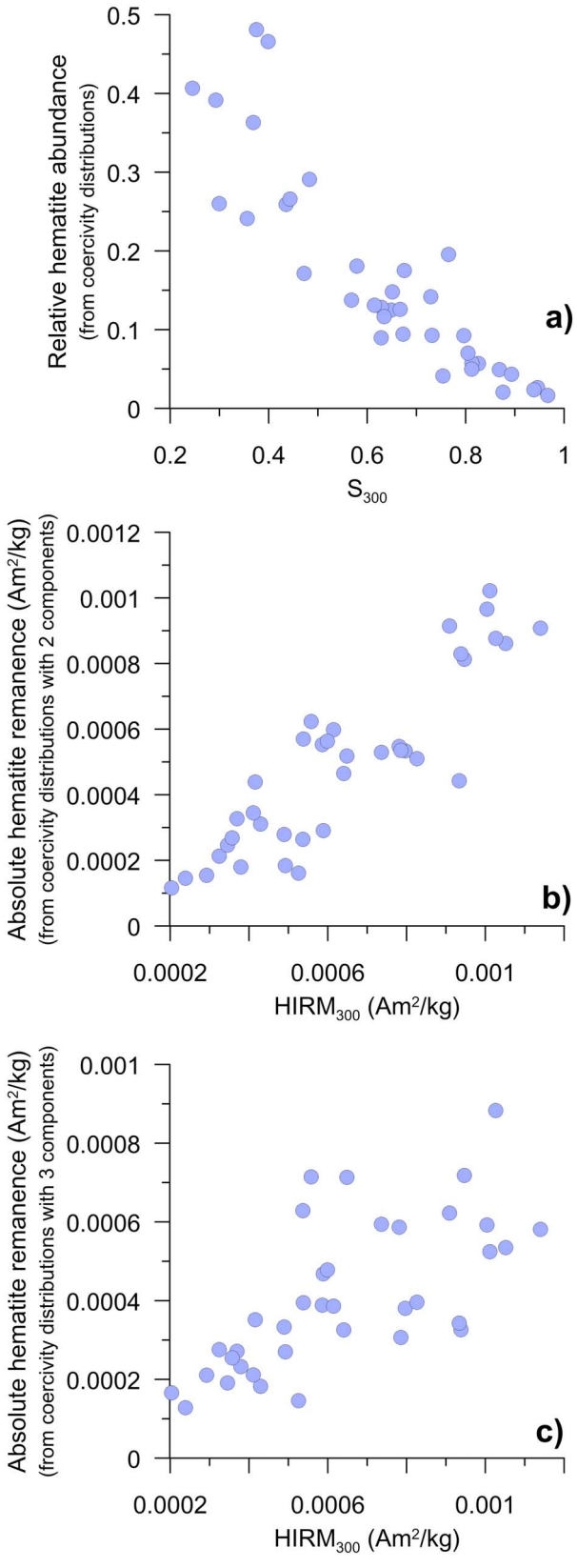

than single-valued parameters such as HIRM or S-ratios. Our comparisons indicate that both techniques yield comparable results (Figure 10), which confirms the usefulness of simple HIRM measurements when estimating hematite abundance even when the corresponding L-ratios are highly variable. A two-component fit (which gave the best correlation between coercivity-distribution-based and HIRM-based estimates) separates the coercivity spectra into two low- and high-coercivity components that are fairly well defined (narrow range of B_h and D_p values) and well separated from each other (Figure 11b). A three-component fit of the coercivity data improves the overall quality of the fit, but these improvements are most pronounced for the low-coercivity part of the spectrum ($B < 5$ mT). The mid- and high-coercivity part of the spectrum is well characterized by two coercivity distributions. The distinct separation and relative homogeneity of these two distributions may be the reason why all techniques yield comparable results. Our analyses suggest that the abundance of hematite is reasonably well quantified using HIRM and S-ratios even when L-ratios are not constant, and it appears that all proxies for hematite abundance (HIRM, analysis of coercivity distributions) reflect true changes in the abundance of hematite in the studied soil profiles.

4. Conclusions

[31] We have demonstrated that the magnetic properties of pre-Bull Lake soil profiles have little magnetic enhancement. In the late and early Bull Lake profiles (soil age 100 and 130 ka) magnetic susceptibility and ARM/IRM increase in the upper soil horizons, similar to soils studied elsewhere, for example, from the Chinese Loess Plateau or the Midwestern United States. Magnetic enhancement appears to have occurred slowly, with no enhancement before a soil age of 100 ka. There is no simple relationship between soil age and the degree of

Figure 10. Comparison of hematite abundance estimates from S_{300mT}, $HIRM_{300}$ and coercivity distributions. (a) Relative abundance estimates from coercivity distributions versus S-ratio. (b) Absolute remanence contributions carried by hematite based on a two-component (high- and low coercivity component) fit of the coercivity distributions shown in Figures 1–5 versus $HIRM_{300}$. (c) Absolute remanence contributions carried by hematite versus $HIRM_{300}$ but with coercivity distributions analyzed using a three-component (high-, medium- low-coercivity) fit.

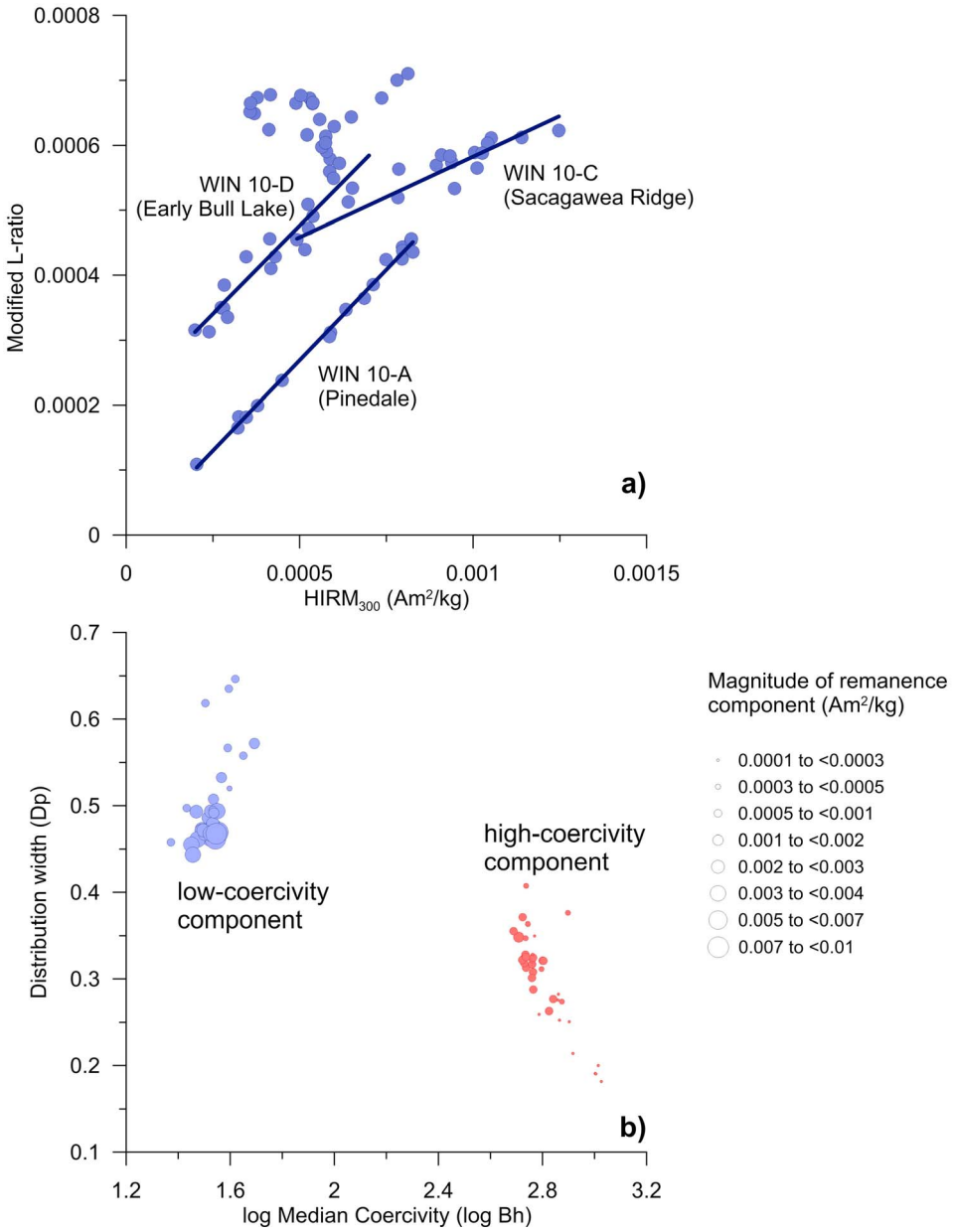

Figure 11. (a) Modified L-ratio [*Liu et al.*, 2007] versus $HIRM_{300}$ for all samples. Linear trends for specific sites are indicated on the graph. (b) Distribution width (D_p) versus log median coercivity (log B_h) for the modeled low- (pale blue symbols) and high-coercivity (pale red symbols) components as determined from a two-component fit analysis of magnetic coercivity distributions. Absolute remanence carried by these components is indicated by increasing symbol size.

magnetic enhancement, and enhancement trends do not extend to our oldest (610–730 ka) soil profile (Sacajawea Ridge, WIN10C). Deflation over long time-scales may have stripped the fine-grained, magnetically enhanced topsoil of the Sacajawea Ridge profile. With respect to age from the Pinedale through Sacajawea Ridge profiles, a loss of ferrimagnets and an increase in hematite occurred (Figure 8).

[32] The soils investigated in this study formed in coarse-grained fluvial deposits. The observed low rates of magnetic enhancement suggest that any equilibrium between climate and soil-magnetic properties is achieved much more slowly than in soils that developed under similar climatic conditions in loess [e.g., *Maher and Hu*, 2006], which severely limits the use of similar paleosols records for quantitative reconstructions of rapid climate

change even if high sedimentation rates allowed for the formation of multiple paleosols. It is unlikely that the magnetic properties of such rapidly buried soils reached equilibrium with the climatic conditions under which they formed.

[33] The observed increase in hematite suggests that pedogenic magnetite may only be an intermediate product in the conversion of iron-bearing minerals to antiferromagnets, with hematite as the stable end product, as suggested by *Torrent et al.* [2006]. However, our findings are also compatible with the magnetic enhancement model of *Balsam et al.* [2004], which predicts the formation of hematite under hot and dry climatic conditions with negligible formation of ferrimagnetic iron oxides.

[34] Our comparison of several hematite abundance proxies demonstrates that HIRM, S-ratios and magnetic coercivity distributions all indicate an increase in absolute and relative accumulation of hematite with soil age. It appears that HIRM can quantify actual increases in hematite abundance even though the modified L-ratio is not constant for these soil profiles and is well suited for rapid, semiquantitative determinations of hematite abundance.

Acknowledgments

[35] This study was funded through a Trinity College Faculty Research Grant to CEG. Trinity College's analytical facilities are supported by grants from the National Science Foundation (MRI-EAR 0923043, MRI-CHE 0959526). The manuscript was significantly improved by the thoughtful comments by the associate editor, A. Roberts, R. Egli as well as a second anonymous reviewer.

References

Balsam, W., J. Ji, and J. Chen (2004), Climatic interpretation of the Luochuan and Lingtai loess sections, China, based on changing iron oxide mineralogy and magnetic susceptibility, *Earth Planet. Sci. Lett.*, *223*, 335–348, doi:10.1016/j.epsl.2004.04.023.

Barrón, V., and J. Torrent (2002), Evidence for a simple pathway to maghemite in Earth and Mars soils, *Geochim. Cosmochim. Acta*, *66*(15), 2801–2806, doi:10.1016/S0016-7037(02)00876-1.

Blundell, A., J. A. Dearing, J. F. Boyle, and J. A. Hannam (2009), Controlling factors for the spatial variability of soil magnetic susceptibility across England and Wales, *Earth Sci. Rev.*, *95*(3–4), 158–188, doi:10.1016/j.earscirev.2009.05.001.

Channell, J. E. T., and C. Mc Cabe (1994), Comparison of magnetic hysteresis parameters of unremagnetized and remagnetized limestones, *J. Geophys. Res.*, *99*(B3), 4613–4623, doi:10.1029/93JB02578.

Dahms, D. E. (2004), Glacial limits in the middle and southern Rocky Mountains, U.S.A., south of the Yellowstone Ice Cap, in *Quaternary Glaciations–Extent and Chronology, Part II*, edited by J. Ehlers and P. L. Gibbard, pp. 275–288, Elsevier, Amsterdam.

Day, R., M. Fuller, and V. A. Schmidt (1977), Hysteresis properties of titanomagnetites: Grain-size and compositional dependence, *Phys. Earth Planet. Inter.*, *13*, 260–267, doi:10.1016/0031-9201(77)90108-X.

Dean, W. E. (1974), Determination of carbonate and organic matter in calcareous sediments and sedimentary rocks by loss on ignition: Comparison with other methods, *J. Sediment. Petrol.*, *44*, 242–248.

Dearing, J. A., K. L. Hay, S. M. J. Baban, A. S. Huddleston, E. M. H. Wellington, and P. J. Loveland (1996), Magnetic susceptibility of soil: An evaluation of conflicting theories using a national data set, *Geophys. J. Int.*, *127*, 728–734, doi:10.1111/j.1365-246X.1996.tb04051.x.

Dearing, J. A., A. Brauer, Y. Hu, P. Doody, and P. A. James (2001), Preliminary reconstruction of sediment-source linkages for the past 6000 yrs at the petit lac d'annecy, france, based on mineral magnetic data, *J. Paleolimnol.*, *25*(2), 245–258, doi:10.1023/A:1008186501993.

Dunlop, D. J. (2002), Theory and application of the Day plot (M_{rs}/M_s versus H_{cr}/H_c): 1. Theoretical curves and tests using titanomagnetite data, *J. Geophys. Res.*, *107*(B3), 2056, doi:10.1029/2001JB000486.

Egli, R. (2004), Characterization of individual rock magnetic components by analysis of remanence curves, 1. Unmixing natural sediments, *Stud. Geophys. Geod.*, *48*, 391–446, doi:10.1023/B:SGEG.0000020839.45304.6d.

Geiss, C. E., and C. W. Zanner (2007), Sediment magnetic signature of climate in modern loessic soils from the Great Plains, *Quat. Int.*, *162–163*, 97–110, doi:10.1016/j.quaint.2006.10.035.

Geiss, C. E., R. Egli, and C. W. Zanner (2008), Direct estimates of pedogenic magnetite as a tool to reconstruct past climates from buried soils, *J. Geophys. Res.*, *113*, B11102, doi:10.1029/2008JB005669.

Geiss, C. E., L. D. Urbano, and C. M. Munroe (2009), Rates of magnetic enhancement in loessic soils estimated from profiles of rapidly eroding soils, *Eos Trans. AGU Fall Meet. Suppl.*, *90*(52), Abstract GP41C-07.

Grimley, D. A., L. R. Follmer, R. E. Hughes, and P. A. Solheid (2003), Modern, Sangamon and Yarmouth soil development in loess of unglaciated southwestern Illinois, *Quat. Sci. Rev.*, *22*, 225–244, doi:10.1016/S0277-3791(02)00039-2.

Grimley, D. A., N. K. Arruda, and M. W. Bramstedt (2004), Using magnetic susceptibility to facilitate more rapid, reproducible and precise delineation of hydric soils in the midwestern USA, *Catena*, *58*(2), 183–213.

Grimley, D. A., J. S. Wang, J. O. Dawson, and D. A. Liebert (2008), Soil magnetic susceptibility: A quantitative proxy of soil drainage for use in ecological restoration, *Restor. Ecol.*, *16*(4), 657–667, doi:10.1111/j.1526-100X.2008.00479.x.

Hall, R. D. (1999), Effects of climate change on soils in glacial deposits, Wind River basin, Wyoming, *Quat. Res.*, *51*, 248–261, doi:10.1006/qres.1999.2032.

Han, J., H. Lu, N. Wu, and Z. Guo (1996), The magnetic susceptibility of modern soils in China and its use for paleoclimate reconstruction, *Stud. Geophys. Geod.*, *40*, 262–275, doi:10.1007/BF02300742.

Hao, Q., F. Oldfield, J. Bloemendal, and Z. Guo (2008), The magnetic properties of loess and paleosol samples from the Chinese Loess Plateau spanning the last 22 million years, *Palaeogeogr. Palaeoclimatol. Palaeoecol.*, *260*, 389–404, doi:10.1016/j.palaeo.2007.11.010.

Heller, F., and T. S. Liu (1986), Paleoclimatic and sedimentary history from magnetic susceptibility of loess in China, *Geophys. Res. Lett.*, *13*, 1169–1172, doi:10.1029/GL013i011p01169.

Ji, J., W. L. Balsam, and J. Chen (2001), Mineralogic and climatic interpretations of the Luochuan loess section (China) based on diffuse reflectance spectrophotometry, *Quat. Res.*, *56*, 23–30, doi:10.1006/qres.2001.2238.

Kukla, G., F. Heller, X. M. Liu, T. C. Xu, T. S. Liu, and Z. S. An (1988), Pleistocene climates in China dated by magnetic susceptibility, *Geology*, *16*, 811–814, doi:10.1130/0091-7613(1988)016<0811:PCICDB>2.3.CO;2.

Liu, Q., A. P. Roberts, J. Torrent, C.-S. Horng, and J. C. Larrasoaña (2007), What do the HIRM and S-ratio really measure in environmental magnetism?, *Geochem. Geophys. Geosyst.*, *8*, Q09011, doi:10.1029/2007GC001717.

Liu, Q., P. X. Hu, J. Torrent, V. Barron, and X. Y. Zhao (2010), Environmental magnetic study of a Xeralf chronosequence in northwestern Spain: Indications for pedogenesis, *Palaeogeogr. Palaeoclimatol. Palaeoecol.*, *293*, 144–156, doi:10.1016/j.palaeo.2010.05.008.

Lyons, R., F. Oldfield, and E. Williams (2010), Mineral magnetic properties of surface soils and sands across four North African transects and links to climatic gradients, *Geochem. Geophys. Geosyst.*, *11*, Q08023, doi:10.1029/2010GC003183.

Maher, B. A. (2011), The magnetic properties of Quaternary aeolian dusts and sediments and their palaeoclimatic significance, *Aeolian. Res.*, *3*(2), 87–144, doi:10.1016/j.aeolia.2011.01.005.

Maher, B. A., and M. Hu (2006), A high-resolution record of Holocene rainfall variations from the western Chinese Loess Plateau: Antiphase behaviour of the African/Indian and East Asian summer monsoons, *Holocene*, *16*(3), 309–319, doi:10.1191/0959683606hl929rp.

Maher, B. A., and R. Thompson (1995), Paleorainfall reconstructions from pedogenic magnetic susceptibility variations in the Chinese loess and paleosols, *Quat. Res.*, *44*, 383–391, doi:10.1006/qres.1995.1083.

Maher, B. A., and R. Thompson (1999), Palaeomonsoons I: The magnetic record of palaeoclimate in the terrestrial loess and palaeosol sequences, in *Quaternary Climates, Environments and Magnetism*, edited by B. A. Maher and R. Thompson, pp. 81–125, Cambridge Univ. Press, Cambridge, U. K., doi:10.1017/CBO9780511535635.004.

Maher, B. A., A. Alekseev, and T. Alekseeva (2003a), Magnetic mineralogy of soils across the Russian Steppe: Climatic dependence of pedogenic magnetite formation, *Palaeogeogr. Palaeoclimatol. Palaeoecol.*, *201*(3–4), 321–341, doi:10.1016/S0031-0182(03)00618-7.

Maher, B. A., H.-M. Yu, H. M. Roberts, and A. G. Wintle (2003b), Holocene loess accumulation and soil development at the western edge of the Chinese Loess Plateau: Implications for magnetic proxies of paleorainfall, *Quat. Sci. Rev.*, *22*, 445–451, doi:10.1016/S0277-3791(02)00188-9.

Orgeira, M. J., R. Egli, and R. H. Compagnucci (2011), A quantitative model of magnetic enhancement in loessic soils, in *Magnetic Earth's Interior*, edited by E. Petrovsky, D. Ivers, T. Harinarayana, and E. Herrero-Bervera, pp. 361–397, Springer, Dordrecht, Netherlands, doi:10.1007/978-94-007-0323-0_25.

Roberts, A. P., Y.-L. Cui, and K. L. Verosub (1995), Wasp-waisted hysteresis loops: Mineral magnetic characteristics and discrimination of components in mixed magnetic systems, *J. Geophys. Res.*, *100*, 17,909–17,924, doi:10.1029/95JB00672.

Robertson, D. J., and D. E. France (1994), Discrimination of remanence-carrying minerals in mixtures, using isothermal remanent magnetization acquisition curves, *Phys. Earth Planet. Inter.*, *82*, 223–234, doi:10.1016/0031-9201(94)90074-4.

Singer, M. J., and P. Fine (1989), Pedogenic factors affecting magnetic susceptibility of northern California soils, *Soil Sci. Soc. Am. J.*, *53*, 1119–1127, doi:10.2136/sssaj1989.03615995005300040023x.

Singer, M. J., P. Fine, K. L. Verosub, and O. A. Chadwick (1992), Time dependence of magnetic susceptibility of soil chronosequences on the California coast, *Quat. Res.*, *37*, 323–332, doi:10.1016/0033-5894(92)90070-Y.

Soil Survey Division Staff (1993), *Soil Survey Manual*, 437 pp., U.S. Gov. Print. Off., Washington, D. C.

Spassov, S., L. P. Yue, D. K. Nourgaliev, F. Heller, R. Kretzschmar, and M. E. Evans (2003), Detrital and pedogenic magnetic mineral phases in the loess/palaeosol sequence at Lingtai (Central Chinese Loess Plateau), *Phys. Earth Planet. Inter.*, *140*(4), 255–275, doi:10.1016/j.pepi.2003.09.003.

Tauxe, L., T. A. T. Mullender, and T. Pick (1996), Potbellies, wasp-waists, and superparamagnetism in magnetic hysteresis, *J. Geophys. Res.*, *101*, 571–583, doi:10.1029/95JB03041.

Torrent, J., V. Barrón, and Q. Liu (2006), Magnetic enhancement is linked to and precedes hematite formation in aerobic soil, *Geophys. Res. Lett.*, *33*, L02401, doi:10.1029/2005GL024818.

Torrent, J., V. Barron, and Q. S. Liu (2010), Magnetic minerals in Calcic Luvisols (Chromic) developed in a warm Mediterranean region of Spain: Origin and paleoenvironmental significance, *Geoderma*, *154*(3–4), 465–472, doi:10.1016/j.geoderma.2008.06.020.

Vidic, N. J., M. J. Singer, and K. L. Verosub (2004), Duration dependence of magnetic susceptibility enhancement in the Chinese loess-palaeosols of the past 620 ky, *Palaeogeogr. Palaeoclimatol. Palaeoecol.*, *211*(3–4), 271–288, doi:10.1016/j.palaeo.2004.05.012.

Virina, E. I., S. S. Faustov, and F. Heller (2000), Magnetism of loess-paleosol formations in relation to soil-forming and sedimentary processes, *Phys. Chem. Earth*, *25*, 475–478, doi:10.1016/S1464-1895(00)00073-9.

Young, J. F. (1981), *Soil Survey of Freemont County, Wyoming, Lander Area*, U.S. Dept. of Agric. Soil Conservation Serv., Washington D. C.